# Steady Axi-symmetric Flow due to Differential Heating in a Rotating Annulus and Its Dependence on Experimental Parameters

**By Seiji Sugata and Shigeo Yoden**
Department of Geophysics, Kyoto University, Kyoto 606-01, Japan

*(Manuscript received 30 April 1992, in revised form 18 August 1992)*

Journal of the Meteorological Society of Japan
Vol. 70, No. 5
Meteorological Society of Japan

# Steady Axi-symmetric Flow due to Differential Heating in a Rotating Annulus and Its Dependence on Experimental Parameters

By Seiji Sugata and Shigeo Yoden

*Department of Geophysics, Kyoto University, Kyoto 606-01, Japan*
*(Manuscript received 30 April 1992, in revised form 18 August 1992)*

## Abstract

Steady axi-symmetric flow in a rotating annulus with differential heating is computed with a high-resolution full-non-linear model in two dimensions. The velocity and temperature fields are investigated for a wide range of external parameters, and their dependence on the parameters is discussed.

A simple diagnostic model of the steady axi-symmetric flow is constructed to understand intuitively how the velocity and temperature fields are determined for given external parameters. The model is applicable to both the conduction-dominated flow and convection-dominated flow, and explains qualitatively how the heat transfer process is determined in each flow. Moreover, the model gives several important quantities characterizing the axi-symmetric flow, such as the intensity of the meridional circulation, that of the zonal flow and the horizontal temperature difference in the interior, for a wide range of the parameters. The results in the simple model agree well with those obtained in the full-non-linear model.

## 1. Introduction

Schneider and Lindzen (1977) studied axi-symmetric flows on a rotating sphere driven by radiation and heat sources due to cumulus convection using a linearized numerical model. They showed that the cumulus heating and friction drive an axi-symmetric meridional circulation in the tropics comparable to the observed Hadley cell circulation. Schneider (1977) introduced a simple approximation to evaluate the intensity and the meridional extent of the Hadley circulation. Held and How (1980) explored Schneider's approach in a wide range of parameters and showed that detailed numerical results could be replicated by the application of some simple balances for the zonal angular momentum and the thermal energy. These studies of axi-symmetric flow give fundamental insights into the nature of the general circulation of the atmosphere.

Rotating annulus experiments with differential heating in the radial direction have been done to understand the basic dynamics of the general circulation of the atmosphere (*e.g.*, Hide and Mason, 1975). Some of the essential factors which determine the general circulation of the atmosphere are included in the rotating annulus experiments, such as rotation, differential heating and gravity, although other factors, such as spherical geometry, surface topography and radiative cooling, are not. These exclusions of the factors make it easier to understand the basic dynamics of the thermal convection in a rotating fluid with the differential heating. In addition, the flow is more tractable over a wide range of experimental parameters and its pattern is more reproducible in the laboratory experiment.

Several régimes of flow are observed in the experiment; steady axi-symmetric flow, steady waves, vacillation and irregular flow. The axi-symmetric flow has the same spatial symmetry as the external forcing (the axi-symmetric heating), while other régimes have zonal (azimuthal) dependence. Selection of the régimes depends on the experimental parameters. On a régime diagram with a logarithm of Taylor number ($Ta$) as the abscissa and that of thermal Rossby number ($Ro_T$) as the ordinate, the axi-symmetric flow is found outside the anvil-shaped region (heavy solid line in Fig. 1) for the case of water (Fowlis and Hide, 1965). The axi-symmetric régime is divided into upper and lower symmetric régimes.

Some theoretical studies of the axi-symmetric flow in the experiment have been done with a top boundary condition of a rigid lid. Hunter (1967) analytically obtained the axi-symmetric flow in the lower symmetric régime, where both of $Ta$ and $Ro_T$ are

©1992, Meteorological Society of Japan

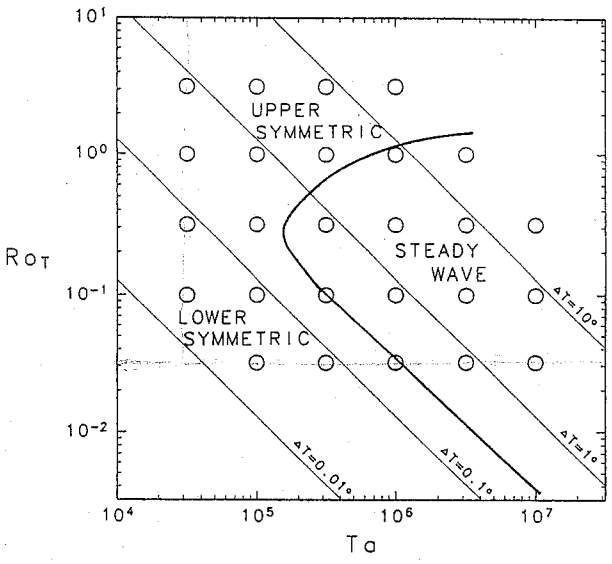


Fig. 1. Régime diagram obtained by Fowlis and Hide (1965) experimentally. The heavy solid line is the transition curve from an axi-symmetric flow régime to a wave régime. Circles indicate the points where axi-symmetric flows are computed.

small, on the assumption that the heat transfer is purely conductive. From this assumption, the temperature field is primarily determined as a solution of the thermal equation. In the interior region, zonal flow is in the thermal wind balance with the temperature field. On the other hand, viscosity plays an important rôle near the boundaries. The Ekman layer is formed in contact with the top and bottom boundaries, while the flow in the side boundary layers is determined as a balance among the viscosity, buoyancy, and Coriolis forces.

McIntyre (1968) analyzed the axi-symmetric flow in the upper symmetric régime on the assumption that the convection is predominant in the heat transfer. Flow in the top and bottom Ekman layers and in the side boundary layers is determined separately, if two integral constants on the temperature field and a constant on the circulation are given appropriately. In determining the constants, he used the thermal wind relation in the interior region and assumed that the top and bottom of the interior are isothermal, respectively. The flow he obtained is quantitatively similar to the numerical results of Williams (1967a, b), who computed the axi-symmetric flows at five points near the transition curve in the régime diagram by integrating the full-non-linear two-dimensional Navier-Stokes equations.

In this study, we compute steady axi-symmetric flows following Williams (1967a, b) for a wide range of the parameters, $Ta$ and $Ro_T$, to investigate the velocity and temperature fields and their dependence on the parameters. The parameter range covers both the upper and lower symmetric régimes, and the wave régime as well. Although the axi-symmetric flow in the wave régime is unstable to wave perturbations (Lorenz, 1962, 1963), it is worth studying to understand the selection of flow régimes. It remains for our future study to compare such axi-symmetric solutions with wave solutions using the same parameters. Moreover, we construct a simple diagnostic model for the axi-symmetric flow in order to understand how the flow field is in equilibrium for given external parameters and how the heat transfer processes depend on the parameters. The simple model is applicable to both the conduction-dominated flow and the convection-dominated flow. Under the constraints of the heat balance, the momentum balance and the thermal wind balance, the model describes relationships among three variables which characterize the axi-symmetric flow: intensity of meridional circulation, zonal flow, and radial temperature difference across the interior. We investigate how the variables depend on the experimental parameters and to what degree their dependence agrees with those of the numerical results.

## 2. Non-linear steady solutions

We consider a fluid, water in this study, contained between two coaxial cylinders of inner and outer radii $a$ and $b$, and two parallel horizontal planes of depth $H$. The dimensions are $a=3.48$ cm, $b=6.02$ cm and $H=5.00$ cm, which are the same as those in the laboratory experiment by Fowlis and Hide (1965). All four bounding surfaces are rigid and the surface of the fluid is in direct contact with the upper lid. The container rotates at a constant rate $\Omega$. The inner and outer walls are held at different constant temperatures, $T_a$ and $T_b$ ($T_a<T_b$), to maintain the difference $\Delta T$. The top and bottom boundaries are thermally insulating. Controllable experimental parameters are $\Omega$ and $\Delta T$. Physical parameters of water are assumed to be constant: the kinematic viscosity, $\nu=1.01\times10^{-2}$ cm$^2$ sec$^{-1}$; the thermometric conductivity, $\kappa=1.41\times10^{-3}$ cm$^2$ sec$^{-1}$; the coefficient of volume expansion, $\alpha=2.06\times10^{-4}$K$^{-1}$. Traditionally the following non-dimensional parameters have been used for the study of rotating annulus experiments: Taylor number, $Ta=4\Omega^2(b-a)^5/\nu^2H$; thermal Rossby number, $Ro_T=gH\alpha\Delta T/\Omega^2(b-a)^2$; Prandtl number, $Pr=\nu/\kappa$; and the aspect ratio $\Gamma=(b-a)/H$, where $g$ is the acceleration of the gravity.

The numerical method described in Sugata and Yoden (1991) is used to obtain steady axi-symmetric flows. The method is basically the same as that in Williams (1967a), except for the modified Boussinesq approximation with an effect due to centrifugal force, although this effect is negligibly small in the present study. The number of grid points used in this study is 65 (horizontal direction) × 129 (verti-

cal direction). The flow is regarded as steady state when variables converge to satisfy the following condition:

$$\left(\frac{\sum_{\text{all grids}}(\partial\theta/\partial t)^2}{\sum_{\text{all grids}}\theta^2}\right)^{1/2} < 10^{-6}.$$

The time required to converge is 30 minutes in physical time at the most. The obtained steady flow at one point in the parameter space is used as an initial condition for the next computation at a neighboring point.

Axi-symmetric flow is obtained for 26 cases at $Ta=10^{4.5}\sim10^{7}$ and $Ro_T=10^{-1.5}\sim10^{0.5}$ except for some points with unrealistically large or small values of $\Delta T$, which are shown in the régime diagram of Fig. 1. The heavy solid line in the figure is the transition curve from the axi-symmetric flow régime to the wave régime (Fowlis and Hide, 1965). Although the curve was obtained in the experiment with a free surface, the transition curve for a rigid lid is expected to be similar to this curve, as shown by Tokioka (1970) theoretically. Therefore, nearly half of the axi-symmetric flows we obtained are expected to be unstable with respect to wave perturbations.

The spatial structure of the velocity field is shown in Figs. 2 and 3. Figure 2 shows streamfunctions of the meridional circulation for 26 cases; strong direct meridional circulation is confined in boundary layers and motion is weak in the interior region. The thickness of the top and bottom (Ekman) boundary layers depends on $Ta$ and that of the side boundary layers mainly depends on $\Delta T$. The intensity of the meridional circulation depends on both $Ta$ and $Ro_T$; the circulation is intensive for large $Ta$ and large $Ro_T$. (Note that the scaling factor is different among the cross sections and indicated above each one). As for the circulation in the interior, two secondary cells and a weak but clear indirect cell are observed for the cases of large $Ta$ and small $Ro_T$. Two secondary cells are observed for the cases of medium and large $Ro_T$, and a single direct cell for the cases of small $Ta$. (See cases D1, A2 and C2 in Williams, 1967b.)

Figure 3 shows cross sections of the zonal velocity for 26 cases. For large $Ta$ and large $Ro_T$, the zonal flow is strong, and therefore both vertical shear and horizontal shear are also large. (Again be careful of the scaling factor.) In each cross section, the maximum value of positive zonal flow near the top boundary is larger than that of negative zonal flow near the bottom, and the position of the former is closer to the inner wall than that of the latter. As $Ta$ increases, positions of the extremes shift inward and slope of the zero line becomes large.

A couple of measures which characterize the intensity of the axi-symmetric flow are introduced; the maximum value of the streamfunction at the mean radius is used as a measure of the meridional circulation, and the maximum value of zonal velocity as a measure of its intensity. Quantitative dependence of these measures on the two parameters, $Ta$ and $Ro_T$, is shown in Fig. 4. Isolines of the measure of meridional circulation (a) have negative gradient in the ($\log Ta$, $\log Ro_T$)-plane, which is less steep ($=-1/2\sim-1/5$) than that of constant $\Delta T$ ($=-1$). The gradient increases with increasing $Ta$ or increasing $Ro_T$. The intensity also increases as $Ta$ and $Ro_T$ increase, and the increment is roughly exponential of $\log Ta$ and $\log Ro_T$. (Note that the contour interval is in geometrical proportion.) As for the measure of the zonal flow (b), isolines have similar dependence but steeper gradient than those in (a). The gradient is nearly equal to that of constant $\Delta T$ for large $Ro_T$, while it is roughly $-1/2$ for small $Ro_T$.

Figure 5 shows normalized temperature fields for 26 cases; the normalized temperature is defined as $\theta=(T-T_a)/\Delta T$. The thermal structure largely depends on $Ro_T$. For example, slope of the isotherms in the interior is steep for small $Ro_T$, which is indicative of the predominance of heat conduction, while it is gentle for large $Ro_T$, indicative of the predominance of heat convection. Overshoot of the temperature near the side boundary layers at large $Ro_T$ is also indicative of strong convection, or meridional circulation. For large $Ro_T$, the radial gradient of the temperature at the side boundaries is large, particularly in the upper part of the inner wall and the lower part of the outer wall. Therefore the radial heat flux at the walls is large for large $Ro_T$.

Quantitative characteristics of the heat transfer processes are shown in Fig. 6: (a) the Nusselt number $Nu$, which is defined as the ratio of the obtained total heat flux to the ideal purely-conductive heat flux, and (b) fraction of the real heat conduction to the total heat flux. The dependence of $Nu$ on $Ta$ and $Ro_T$ is similar to that of the measure of the meridional circulation in Fig. 4a. That is, isolines have a gradient of $-1/3\sim-1/4$ for small $Ro_T$ in the ($\log Ta$, $\log Ro_T$)-plane, but $-1/2$ or steeper for large $Ro_T$. The magnitude of $Nu$ has a nearly exponential increment with $\log Ta$ and $\log Ro_T$. Figure 6b shows the percentage of the conduction at the mean radius, which is less dependent on $Ta$ than (a). It is large for small $Ro_T$, and the heat transfer is nearly conductive at $Ro_T=10^{-1.5}$. On the other hand, convection is predominant at $Ro_T=10^{0.5}$.

We also investigated the balance in the vorticity equation for the meridional circulation; each term of the vorticity equation (Eq. (7) in Sugata and Yoden (1991)) was computed in the meridional section for 26 cases (figures are not shown). The interior region of the fluid is almost in a thermal wind balance; the buoyancy torque due to radial gradient of the temperature is balanced with the Coriolis torque due to the vertical shear of the zonal flow. The interior

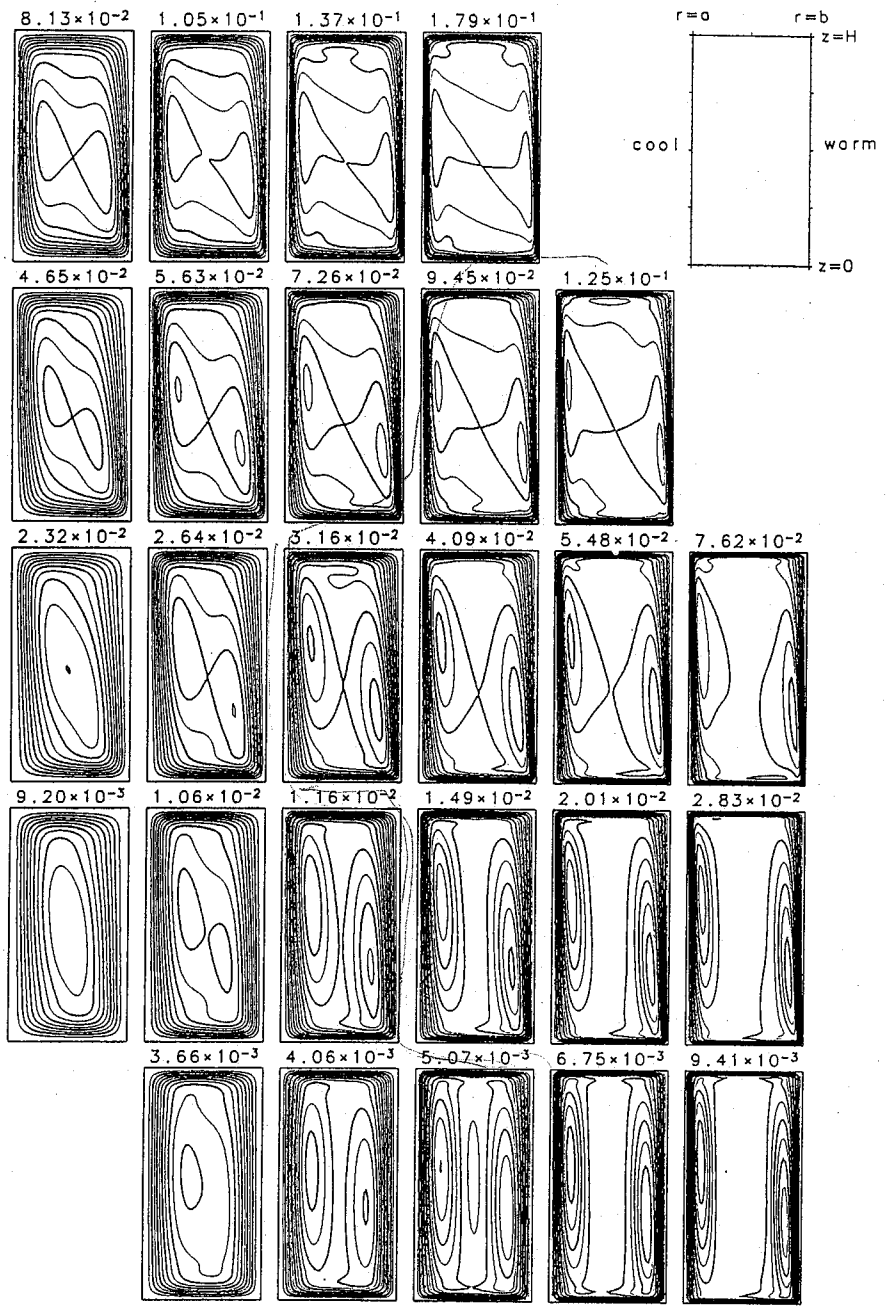


Fig. 2. Streamfunction of the meridional circulation of steady axi-symmetric flows for 26 cases, scaled by its maximum value at the mean radius $r_c=(a+b)/2$. The maximum value is indicated above each cross section with a unit of [cm$^3$/s]. The contour interval is 0.1. The arrangement of cross sections corresponds to that of circles in Fig. 1.

region is small for small $\Delta T$. In the top and bottom boundary layers, the viscosity term is mostly balanced with the Coriolis term, which is indicative of the nature of the Ekman layer. In the side boundary layers, on the other hand, the viscosity term is essentially balanced with the buoyancy term, although the Coriolis term is also significant in the balance for small $Ro_T$.

## 3. Simple diagnostic model

### *3.1 Balance requirements*

A simple diagnostic model is constructed in order to understand intuitively how the flow field obtained in the previous section is determined for given external parameters and how the heat transfer processes depend on the parameters. Several quantities which characterize the flow field are introduced, and their relationships are obtained from rough estimations.

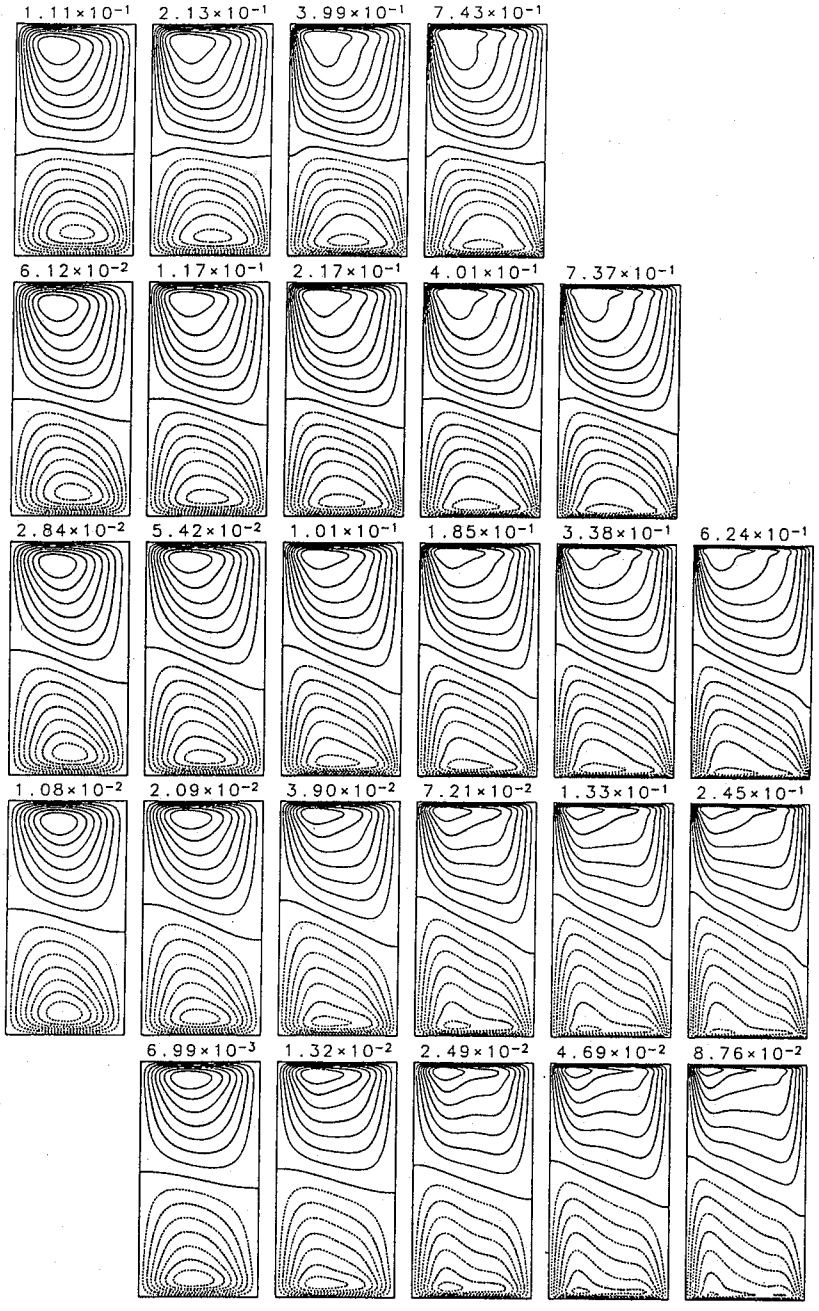


Fig. 3. As in Fig. 2, but for zonal velocity scaled by its maximum value. The maximum value is indicated above each cross section with a unit of [cm/s]. The contour interval is 0.125. Negative values are plotted with dotted lines.

Moreover, the dependence of the quantities on the parameters is discussed in the resulting simple system.

We consider an equilibrium state of the axi-symmetric flow in Cartesian coordinates $(x, y, z)$ instead of the cylindrical coordinates $(r, \lambda, z)$ neglecting the curvature of the annulus: $x=r$, and $y=r_c\lambda$, where $r_c=(a+b)/2$. The corresponding velocity components are $(u, v, w)$, and the meridional circulation is expressed with a streamfunction $\Psi$ as $(u, w)=\frac{1}{r_c}\left(\frac{\partial\Psi}{\partial z}, -\frac{\partial\Psi}{\partial x}\right)$, where the factor $1/r_c$ is useful in comparing the result with that in the previous section. The flow field in the meridional plane of height $H$ and width $L(=b-a)$ is divided into five sections; the top and bottom boundary layers with depth $h$, the inner and outer side boundary layers with width $l$, and the interior region, of which height is then $H_I=H-2h$ and width is $L_I=L-2l$.

Now we introduce several variables which characterize the fundamental properties of the steady axi-symmetric flow. The axi-symmetric flow for the

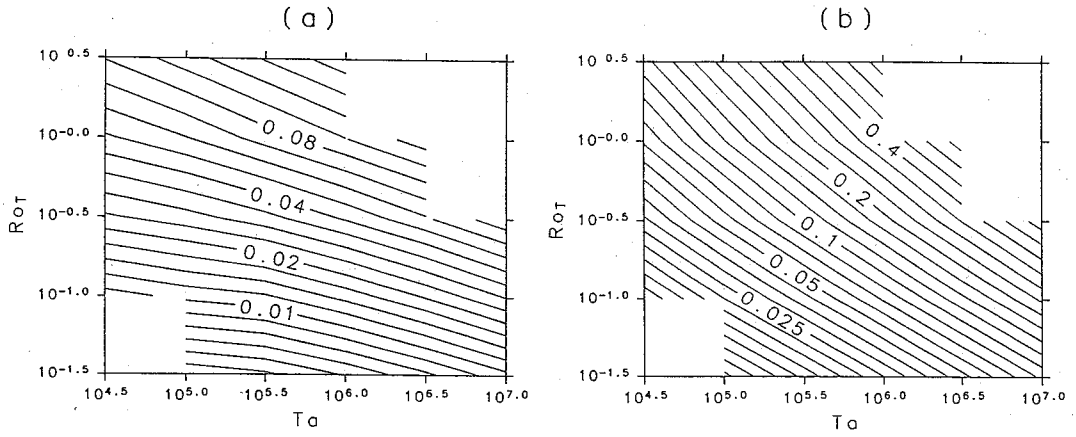


Fig. 4. (a) Dependence of the intensity of meridional circulation of $\log Ta$ and $\log Ro_T$; maximum value of streamfunction [cm$^3$/s] at the mean radius $r_c=(a+b)/2$ of the annulus is adopted as a measure of the intensity. Boundary value of the streamfunction is set to be zero. (b) Dependence of the maximum value of zonal flow [cm/s]. Both contour intervals are in geometrical proportion.

present parameter range is characterized as follows:

1. The meridional circulation is mostly confined to the boundary layers and its intensity is represented by $\Psi_I$, the value of the streamfunction just outside the boundary layers. The quantity $\Psi_I/r_c$ represents the constant meridional volume flux per unit length in $y$ direction.

2. The zonal flow field is characterized by the vertical shear and representative values of the zonal velocity at the top and bottom of the interior, $v_{(t)}$ and $v_{(b)}$, respectively, are introduced. The vertical shear has a magnitude of $(v_{(t)}-v_{(b)})/H_I$.

3. The normalized temperature field is characterized by three variables: an average temperature of the top boundary layer $\theta_{(t)}$, that of the bottom boundary layer $\theta_{(b)}$, and radial difference $\delta\theta$ across the interior region.

The quantities introduced here, $h$, $l$, $\Psi_I$, $v_{(t)}$, $v_{(b)}$, $\theta_{(t)}$, $\theta_{(b)}$ and $\delta\theta$, are determined for given external parameters.

Now we try to find relationships among these quantities and experimental parameters. The top and bottom boundary layers and the Ekman layer for the present parameter range of ($Ta$, $Ro_T$), because the Ekman number is sufficiently small; $\nu/2\Omega H^2 \leq 10^{-3}$. Therefore the depth $h$ is given by the Ekman depth:

$$h=\sqrt{2}\pi h_0, \quad h_0=\sqrt{\nu/2\Omega}. \tag{1}$$

The depth is uniquely determined for a given rotation rate $\Omega$. On the other hand, it is not straightforward to represent the width $l$ of the side boundary layers with the external parameters. By a detailed analysis, McIntyre (1968) estimated the width, which depends on the temperature profile just outside the boundary layer. Here we leave the specification of $l$ for a which. (Afterward we will make a crude assumption on $l$.)

To obtain a relationship between the zonal velocity and the temperature field, we use the thermal wind relation (*cf.* Eq. (4.4) in McIntyre (1968)), which approximately holds in the interior for the present parameter range;

$$\frac{v_{(t)}-v_{(b)}}{H_I}=\frac{g\alpha\Delta T}{2\Omega}\frac{\delta\theta}{L_I}. \tag{2}$$

From the theory of Ekman layer, $v_{(t)}$ and $v_{(b)}$ are related to the meridional circulation $\Psi_I$:

$$v_{(t)}=-v_{(b)}=\frac{\sqrt{2}\Psi_I}{h_0 r_c}. \tag{3}$$

This is the same as Eq. (5.3) in McIntyre (1968) except that radius $r$ is replaced by the mean radius $r_c$. Elimination of $v_{(t)}$ and $v_{(b)}$ between (2) and (3) gives a relationship between $\Psi_I$ and $\delta\theta$;

$$\frac{2\sqrt{2}}{H_I h_0 r_c}\Psi_I=\frac{g\alpha\Delta T}{2\Omega L_I}\delta\theta, \tag{4}$$

which means that the intensity of the meridional circulation is in proportion to the horizontal temperature difference in the interior if $L_I$ is independent of $\Psi_I$ and $\delta\theta$.

In order to obtain another relationship, we consider the heat transfer across the annulus. The inward heat flux integrated from the bottom to the top at any $x$ must be equal in equilibrium states. For $x=a$ and $r_c$,

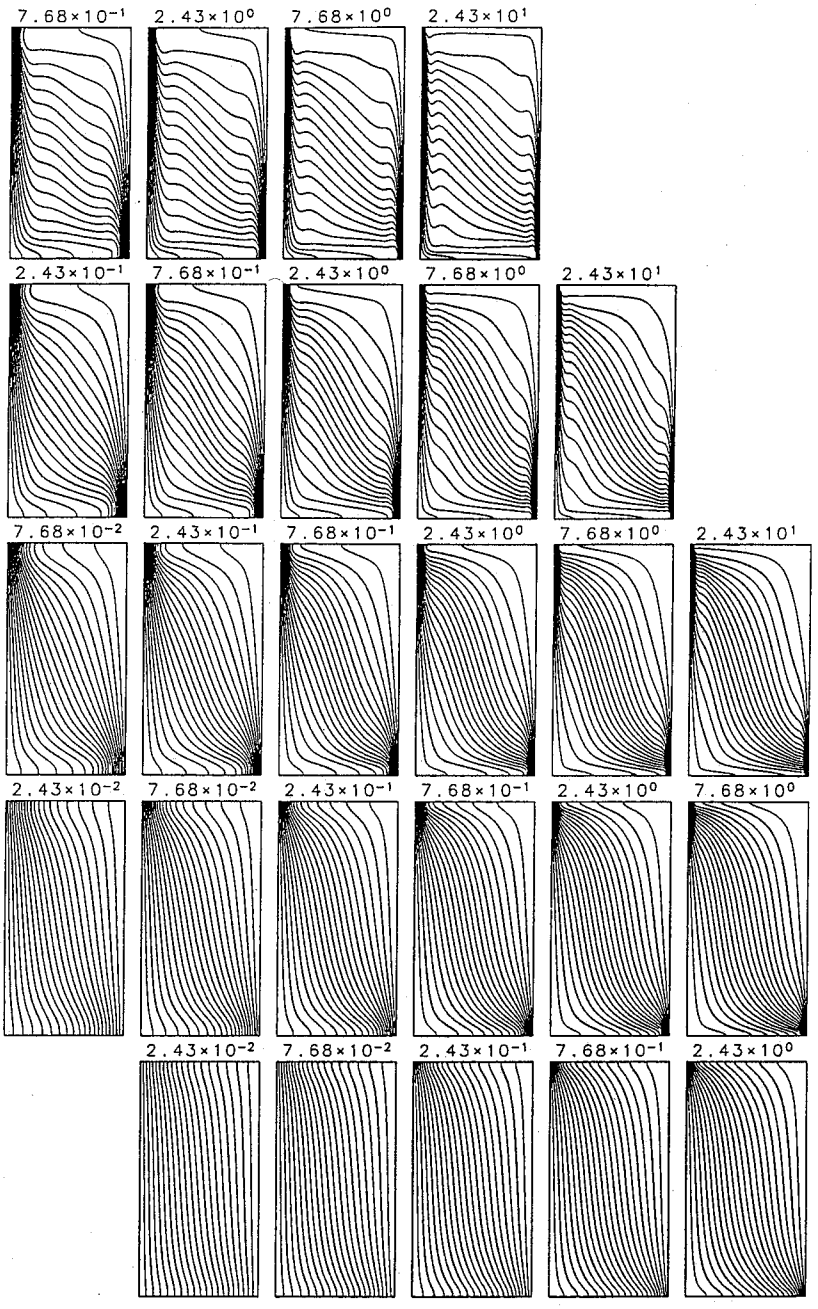


Fig. 5. As in Fig. 2 but for normalized temperature with a contour interval of 0.05. The value indicated above each cross section is $\Delta T$ [K].

$$\Delta T \int_0^H \kappa \left.\frac{\partial \theta}{\partial x}\right|_{x=a} dz = \Delta T \int_0^H \kappa \left.\frac{\partial \theta}{\partial x}\right|_{x=r_c} dz - \Delta T \int_0^H [u\theta]_{x=r_c} dz. \quad (5)$$

That is to say, the heat conduction at the inner wall is equal to the sum of conduction and convection at the mean radius. The heat conduction at the inner wall is estimated as

$$\Delta T \varepsilon \kappa \frac{1-\delta\theta}{2l} H, \quad (6)$$

where $\varepsilon$ is a coefficient expressing the effect of the variation of horizontal temperature gradient in the side boundary layer, which gradually increases toward the wall. If the temperature gradient is constant throughout the layer, $\varepsilon = 1$. The conduction term on the right-hand side (r.h.s.) of (5) is estimated as

$$\Delta T \kappa \frac{\delta\theta}{L_I} H, \quad (7)$$

while the convection term is estimated as

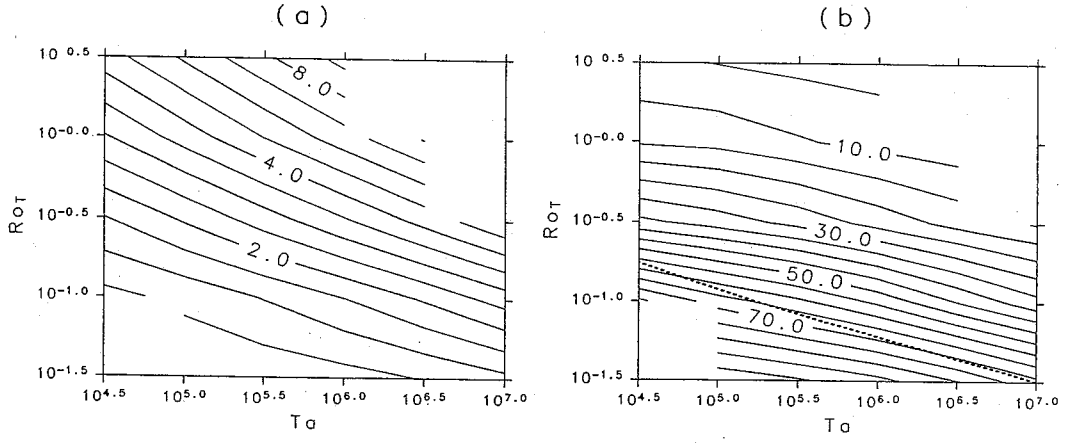


Fig. 6. As in Fig. 4, but for (a) the Nusselt number and (b) percentage of the conductive hear flux in the total heat flux at the mean radius. The contour interval is linear in (b). A thick dash-line in (b) indicates the 50 % line that is estimated from a simple diagnostic model described in Section 3.

$$\Delta T \frac{\Psi_I}{r_c}\left(\theta_{(t)}-\theta_{(b)}\right). \tag{8}$$

By substituting (6)$\sim$(8) into (5), we obtain the following equation;

$$\varepsilon\kappa\frac{1-\delta\theta}{2l}H=\kappa\frac{\delta\theta}{L_I}H+\frac{\Psi_I}{r_c}\left(\theta_{(t)}-\theta_{(b)}\right), \tag{9}$$

which shows a relationship between $\Psi_I$ and $\delta\theta$ opposite to Eq. (4); $\Psi_I$ decreases with increasing $\delta\theta$ if other variables are assumed to be independent of $\Psi_I$ and $\delta\theta$.

The relative importance of the heat conduction and the heat convection at the mean radius is given by the ratio of two terms in the r.h.s. of (9). The ratio $\gamma$ becomes as follows with (4):

$$\gamma\equiv\frac{\text{(conductive heat flux)}}{\text{(convective heat flux)}}=\frac{4\sqrt{2}\kappa H\Omega}{H_I h_0 g\alpha\Delta T}\frac{1}{\theta_{(t)}-\theta_{(b)}}. \tag{10}$$

The ratio is inversely proportional to $\theta_{(t)}-\theta_{(b)}$, which is determined internally for given external parameters. It is clear that $\theta_{(t)}-\theta_{(b)}\sim 0$ for conduction-dominated flow and $\theta_{(t)}-\theta_{(b)}\sim 1$ for convection-dominated flow. In order to estimate the relative importance in the ($\log Ta$, $\log Ro_T$)-plane, a line of $\gamma=1$ is drawn in Fig. 6b (a dotted line) with $\theta_{(t)}-\theta_{(b)}=0.5$. The $\gamma=1$ line is not far from the contour of 50 % in Fig. 6b obtained from the nonlinear results, which is indicative of the usefulness of the present simple model. From Eq. (10), it is clear that convection is dominant ($\gamma\ll 1$) far above the dotted line in Fig. 6b, while conduction is dominant ($\gamma\gg 1$) far below the dotted line.

We need some other relationships or assumptions to close the system, because two Eqs. (4) and (9) still have the following variables; $\Psi_I$, $\delta\theta$, $\theta_{(t)}$, $\theta_{(b)}$ and $L_I$ (or $l$). Now, we consider two extreme cases of convection-dominated flow and conduction-dominated flow, separately.

*3.2 Convection-dominated flow*

In the convection-dominated flow, the conduction term on the r.h.s. of (9) can be neglected, and temperature difference between the top and bottom boundary layers can be set to $\Delta T$ (*i.e.*, $\theta_{(t)}-\theta_{(b)}=1$). The latter assumption "linearizes" the heat convection term. Then the heat transfer equation (9) becomes

$$\frac{\Psi_I}{r_c}=\varepsilon\kappa\frac{1-\delta\theta}{2l}H. \tag{11}$$

Three variables $\Psi_I$, $\delta\theta$ and $L_I$ (or $l$) still remain in (4) and (11).

To close the system, we further assume that the width $l$ of the side boundary layers is determined only by the external parameters from balance requirements in the heat equation and the vorticity equation (see appendix for details):

$$l=2\left(\frac{\nu\kappa H}{g\alpha\Delta T}\right)^{1/4}. \tag{12}$$

Furthermore, the coefficient $\varepsilon$ is set to be 2 in (11) because it is estimated from non-linear solutions that the horizontal temperature gradient at the boundary is about twice as large as that averaged in the boundary layer.

From the above assumptions and estimations, the system of (4) and (11) can be solved for $\Psi_I$ and $\delta\theta$. That is, intensity of the meridional circulation and the temperature difference across the interior are determined for given external parameters. Figure 7a shows the two linear relations (4) and (11) for five values of $Ro_T$ with fixed $Ta=10^6$ and Fig. 7b for

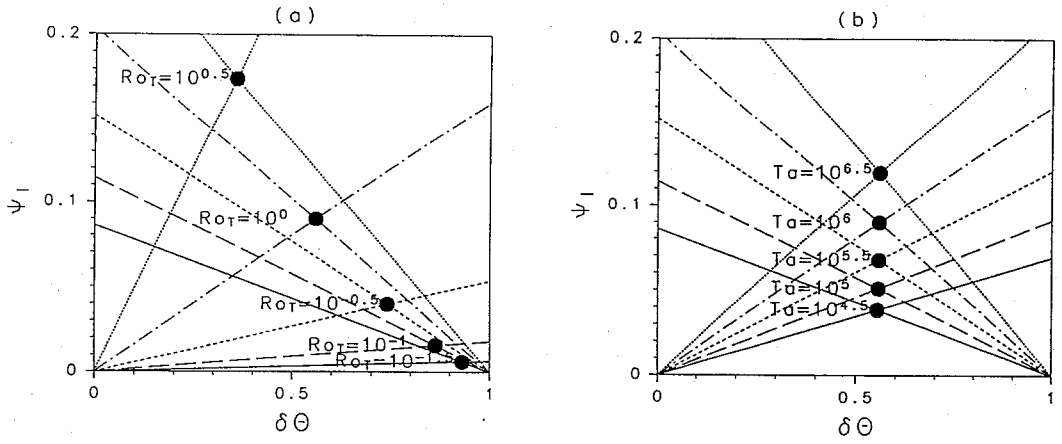


Fig. 7. Two linear relations between the radial temperature difference across the interior $\delta\theta$ and the intensity of meridional circulation $\Psi_I$ [cm$^3$/s] for fixed $Ta$ at $10^6$ (a) and for fixed $Ro_T$ at $10^0$ (b). The intersection of the two lines indicated by • gives an equilibrium solution.

five values of $Ta$ with fixed $Ro_T=10^0$. The intersection denoted by a closed circle gives the equilibrium solution $\Psi_I$ and $\delta\theta$ in the present simple system. The gradient of a line of (4), which is drawn through the origin, depends mainly on the value of $h_0\Delta T/\Omega(\propto \Delta T\Omega^{-3/2} \propto Ro_T Ta^{1/4})$, because $H_I$ $(=H-2h)$ and $L_I$ $(=L-2l)$ do not change very much owing to the smallness of the boundary layers. On the other hand, the gradient of a line of (11) depends only on $l$. Therefore, the negative gradient is nearly in proportion to $\Delta T^{1/4}$. If we fix $Ta$ (, or $\Omega$) and increase $Ro_T$ (, or $\Delta T$) as shown in Fig. 7a, the gradient of (4) increases much faster than that of (11) due to the 1/4-th power. As a result, $\Psi_I$ of the equilibrium solution increases and $\delta\theta$ decreases. On the other hand, if we fix $Ro_T$ and increase $Ta$, both lines of (4) and (11) increase their gradient as $\propto \Omega^{1/2}$ because $\Delta T \propto \Omega^2$ for $Ro_T=$constant. As a result, $\delta\theta$ of the equilibrium solution changes little and $\Psi_I$ increases. The dependence of the two characteristic features on $Ro_T$ and $Ta$ corresponds well to the non-linear solutions in Section 2 (Figs. 2 and 5).

The simultaneous equations (4) and (11) are solved for $\Psi_I$ and $\delta\theta$:

$$\Psi_I = \frac{\varepsilon\kappa H r_c}{2l}\frac{1}{1+f}, \tag{13}$$

$$\delta\theta = \frac{f}{1+f}, \tag{14}$$

where $f=2\sqrt{2}\varepsilon\kappa H L_I\Omega/(lh_0H_Ig\alpha\Delta T)$. A measure of the zonal flow, $v_{(t)}$, is obtained from (3);

$$v_{(t)} = \frac{\varepsilon\kappa H}{\sqrt{2}lh_0}\frac{1}{1+f}. \tag{15}$$

Figure 8 shows the dependence of $\Psi_I$ and $v_{(t)}$ on the two external parameters $Ta$ and $Ro_T$. Note that the assumption of the predominance of convection and the estimation of (12) are valid in the upper part of each figure. The intensity of the meridional circulation $\Psi_I$ shown in Fig. 8a is close to that in Fig. 4a for the non-linear solutions, particularly in the upper part. The intensity of the zonal flow $v_{(t)}$, which is shown in Fig. 8b, corresponds well to that of Fig. 4b. The Nusselt number is defined as $Nu=\Psi_I L/r_c\kappa H$ in this simple model, because the total heat flux equals $\Psi_I\Delta T/r_c$ from Eq. (8) and the ideal purely-conductive heat flux is $\kappa\Delta TH/L$. Hence the figure for $Nu$ is identical to Fig. 8a except for the factor $L/r_c\kappa H$, and not shown here. The similarity between the contours of the intensity of meridional circulation and those of $Nu$ was already pointed out in the previous section for the non-linear solutions (Figs. 4a and 6a). From these results, we conclude that our simple diagnostic model can represent the essential properties of the upper axi-symmetric flow reasonably well.

Now we further investigate the dependence of our solutions on the experimental parameters $\Omega$ and $\Delta T$, or $Ta$ and $Ro_T$. For the present parameter ranges, the boundary layers are estimated to be thin ($h\ll H$ and $l\ll L$) from (1) and (12), and then $L_I/H_I\sim L/H$, which is independent of $\Omega$ and $\Delta T$. Therefore the quantity $f$ in (13)$\sim$(15) is,

$$f = c_1\Omega^{3/2}\Delta T^{-3/4} \tag{16}$$

where $c_1$ is a positive constant which is independent of the parameters $\Omega$ and $\Delta T$. Equations (13)$\sim$(15) become as follows using the definitions of $Ta$ and $Ro_T$;

$$\Psi_I = \frac{c_2\Delta T^{1/4}}{1+c_1\Omega^{3/2}\Delta T^{-3/4}} = \frac{c_2'\,(TaRo_T)^{1/4}}{1+c_1'Ro_T^{-3/4}}, \tag{17}$$

$$\delta\theta = \frac{c_1\Omega^{3/2}\Delta T^{-3/4}}{1+c_1\Omega^{3/2}\Delta T^{-3/4}} = \frac{c_1'Ro_T^{-3/4}}{1+c_1'Ro_T^{-3/4}}, \tag{18}$$

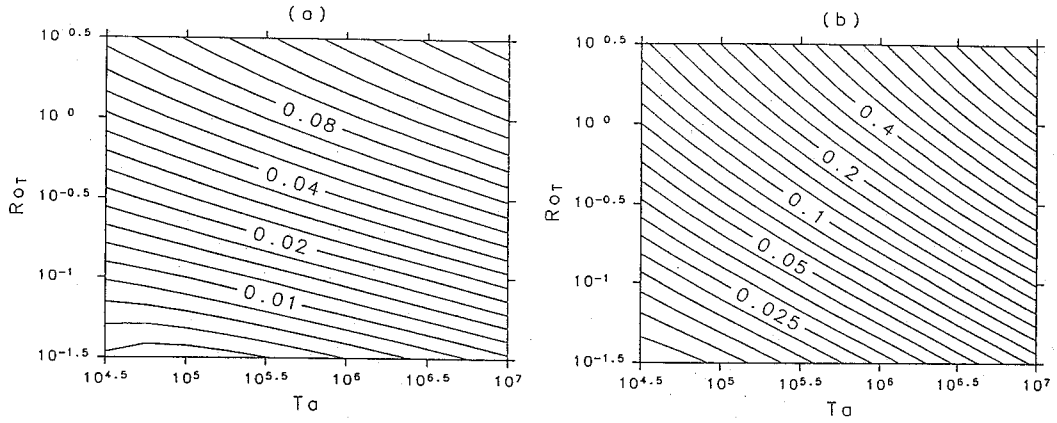


Fig. 8. As in Fig. 4, but for the present simple diagnostic model. (a) intensity of the meridional circulation, $\Psi_I$ [cm$^3$/s]; (b) intensity of the zonal flow, $v_{(t)}$ [cm/s].

$$v_{(t)} = \frac{c_3 \Omega^{1/2} \Delta T^{1/4}}{1 + c_1 \Omega^{3/2} \Delta T^{-3/4}} = \frac{c_3' Ta^{1/2} Ro_T^{1/4}}{1 + c_1' Ro_T^{-3/4}} \propto Ta^{1/4} \Psi_I, \tag{19}$$

where all $c_i$ and $c_i'$ are positive constants. Numerator of the r.h.s. of (17) is constant along a line with $\log Ro_T = -\log Ta + \text{constant}$, which has a gradient of $-1$ in Fig. 8a, and increases from bottom-left to top-right in the figure. On the other hand, the denominator of the r.h.s. of (17) is constant along a horizontal line with $Ro_T = \text{constant}$, and increases from top to bottom. As a result, Eq. (17) gives an outline of the curved contours of $\Psi_I$ shown in Fig. 8a. As for the measure of the zonal flow, Eq. (19) gives an outline of the curved contour shown in Fig. 8b, where gradient of each isoline is steeper than that of $\Psi_I$ due to the factor $Ta^{1/4}$. As shown in Eq. (18), the temperature difference $\delta\theta$ depends only on $Ro_T$ but not on $Ta$. This dependence explains the characteristic thermal structure shown in Fig. 5, where the slope of the isotherms in the interior depends mainly on $Ro_T$.

*3.3 Conduction-dominated flow*

In the conduction-dominated flow, the convection term on the r.h.s. of (9) can be neglected and the parameter $\varepsilon$ can be set to 1. Then the heat transfer equation is reduced to

$$\frac{\delta\theta}{L_I} = \frac{1}{L}. \tag{20}$$

Therefore the side thermal boundary layers do not exist and the thermal wind relation holds across the annulus. The vertical shear is estimated from the thermal wind relation (2), and the zonal flow $v_{(t)}$ is obtained with (3) as follows;

$$v_{(t)} = \frac{g\alpha H_I}{4L} \frac{\Delta T}{\Omega}. \tag{21}$$

The Ekman layer theory gives the relationship (3) between $\Psi_I$ and $v_{(t)}$,

$$\Psi_I = \frac{g\alpha H_I r_c \sqrt{\nu}}{8L} \frac{\Delta T}{\Omega^{3/2}}. \tag{22}$$

Plots of these quantities in the ($\log Ta$, $\log Ro_T$)-plane (not shown) correspond well to those in the lower part of Fig. 4a and 4b.

## 4. Discussion

In the previous section two diagnostic Eqs. (4) and (9) are derived from several balance requirements. They have opposite relation between the intensity of the meridional circulation, $\Psi_I$, and the radial temperature difference across the interior, $\delta\theta$. Here we summarize the physical meaning of the two equations. Equation (4) is based on the thermal wind balance (2) and the mass-transport requirement in the Ekman layer (3). From the thermal wind balance the zonal flow just outside the Ekman layer, $v_{(t)}$, is large for large $\delta\theta$. At the same time, $\Psi_I$ must be large for large $v_{(t)}$ from the mass-transport requirement. As a result, *the intensity of the meridional circulation ($\Psi_I$) must be large for large radial temperature difference ($\delta\theta$)*. On the other hand, Eq. (9) is a balance requirement in the heat budget. If $\delta\theta$ is large, the heat conduction at the side boundaries is small because the temperature gradient in the side boundary layer, $(1-\delta\theta)/2l$, is small. Then the convective heat flux outside the side boundary layers, namely, the last term in (9), must be small because the l.h.s. of (9) is small and the first term in the r.h.s. is not negligible. That is, *the intensity of the meridional circulation ($\Psi_I$) must be small for large radial temperature difference ($\delta\theta$)*. These two balance requirements with opposite relation between $\Psi_I$ and $\delta\theta$ determine $\Psi_I$ and $\delta\theta$ uniquely for given external parameters as shown in Fig. 7 for convection-dominated flow.

The balanced flow that is obtained in this simple diagnostic model has dependence on the external parameters through the coefficients in Eqs. (4) and (11) for convection-dominated flow. The dependence can be divided into two parts; one is the term $\Delta T/\Omega$ in (4) and the other is the thickness of the boundary layers $h$ and $l$, which depends on the external parameters as shown in (1) for the top and bottom boundary layers and (12) for the side boundary layers. Now we set the width and the depth of the boundary layers to be constant in order to focus on the term $\Delta T/\Omega$ in (4). Then Eqs. (17), (18) and (19) become as follows,

$$\Psi_I = \frac{d_2}{1 + d_1 Ta^{-1/2} Ro_T^{-1}}, \tag{23}$$

$$\delta\theta = \frac{d_1}{1 + d_1 Ta^{-1/2} Ro_T^{-1}}, \tag{24}$$

$$v_{(t)} = \frac{d_3}{1 + d_1 Ta^{-1/2} Ro_T^{-1}}, \tag{25}$$

where $d_i$ are positive constants independent of $\Omega$ and $\Delta T$. All of $\Psi_I$, $\delta\theta$ and $v_{(t)}$ depend only on $Ta^{1/2}Ro_T$. Isolines of these measures are straight lines in the ($\log Ta$, $\log Ro_T$)-plane and have a gradient of $-1/2$, which explains very essence of the dependence in Fig. 8, particularly good for $\Psi_I$ (a). That is to say, the term $\Delta T/\Omega$ in the thermal wind relation essentially determines the dependence on the external parameters, and the variation of the boundary-layer thickness modifies it: Owing to the variation of the thickness, gradient of isolines of the meridional circulation becomes gentle, while that of the zonal flow becomes steep.

The simple diagnostic model introduced in this study is based on three equations; the thermal wind equation (2), the Eq. (3) for the mass transport in the Ekman layer, and the heat budget equation (9). It is worthy to point out that (3) is also an equation for the angular momentum budget. At the mean height $z=H/2$, upward angular momentum flux in the outer side boundary layer is estimated as $b^2\Omega \cdot \Psi_I/b$ and downward flux in the inner side boundary layer as $a^2\Omega \cdot \Psi_I/a$, because the zonal flow is almost zero at $z=H/2$. Therefore the net upward flux is $(b-a)\Omega\Psi_I$ at the mean height. In an equilibrium state, it must be compensated by the diffusion at the boundaries in the upper (or lower) half of the container. The diffusion of angular momentum at the upper lid is estimated as $\nu\frac{r_c v_{(t)}}{h}(b-a)$. Therefore $v_{(t)}=\pi\Psi_I/(\sqrt{2}r_c h_0)$ if we neglect the diffusion at the side boundaries, which is small compared with that at the upper lid (see Fig. 3). If we compare this with Eq. (3), only a factor of $\pi/2$ is different. Thus Eq. (3) can be interpreted as an equation for the angular momentum budget.

## 5. Conclusions

Steady axi-symmetric flow in a rotating annulus with differential heating was obtained by numerical time-integrations of the two-dimensional Navier-Stokes equations over a wide range of external parameters. The velocity field of the meridional circulation, the zonal flow and the temperature field are shown at 26 points around the anvil-shaped transition curve in the régime diagram (Figs. 2, 3, and 5). The meridional circulation is mostly confined to thin boundary layers and its intensity is large for large Taylor number ($Ta$) and large thermal Rossby number ($Ro_T$). The width of the side boundary layers and depth of the top and bottom boundary layers depend on these parameters separately. The vertical shear of the zonal flow is large for large $Ta$ and large $Ro_T$. The temperature field is intimately related to the intensity of the meridional circulation, because the circulation has an important role in heat convection in the meridional heat transfer, particularly for large $Ro_T$. Moreover, the temperature field is in the thermal wind balance with the zonal flow in the interior region.

Several quantities which characterize these features of the steady axi-symmetric flow are selected and their dependence on the parameters is clarified quantitatively (Figs. 4 and 6). The intensity of the meridional circulation and the Nusselt number have similar dependence, while the zonal flow has a different dependence.

A simple diagnostic model was constructed to understand intuitively how the flow field is determined for given external parameters. The intensity of the meridional circulation and radial temperature difference across the interior are key variables to characterize the flow field. Two Eqs. (4) and (9), which are the essence of our model, give their relationships under appropriate assumptions; Eq. (4) is the thermal wind relation in the interior with the Ekman layer theory and (9) is the heat transfer equation. Our simple model reproduces the dependence of these quantities on $Ta$ and $Ro_T$ obtained in the full nonlinear computations.

The convection-dominated flow is essentially determined as follows: Zonal flow just outside the Ekman layer must be strong for large radial temperature difference across the interior from the thermal wind balance. At the same time, the meridional circulation must be strong for the strong zonal flow from the mass-transport relation in the Ekman layer. That is, the meridional circulation must be *strong* for a large radial temperature difference across the interior. On the other hand, the heat transfer equation gives an opposite relationship between these quantities. If the radial temperature difference across the interior is large, that across the side boundary layers is small, namely, the heat flux

at the side boundaries is small. Then the convective heat flux outside the side boundary layers must be small from the heat balance requirement. That is, the meridional circulation must be *weak* for a large radial temperature difference across the interior. These two balance requirements with opposite relationships determine the intensity of the meridional circulation and the radial temperature difference across the interior uniquely for given external parameters $Ta$ and $Ro_T$.

On the other hand, the conduction-dominated flow is determined as follows: The temperature field is determined by the heat conduction. Therefore, the side thermal boundary layers do not exist. The zonal flow field is in thermal wind balance with the temperature field. By the Ekman layer theory, the intensity of the meridional circulation is related to the zonal flow at the top and bottom of the interior region.

## Acknowledgments

The authors wish to thank Professor I. Hirota and Dr. S. Sakai for their valuable comments during the work. The GFD-DENNOU Library produced by Drs. M. Shiotani and S. Sakai was used for drawing the figures.

## Appendix

### *Width of the side boundary layer*

McIntyre (1968) showed that the width of the side boundary layer is not strictly determined only by the external parameters. However, it is possible to estimate the width $l$ for the present simple model under several acceptable approximations.

The heat equation in the side boundary layer is approximated as follows (McIntyre, 1968):

$$\frac{\Delta T}{r_c}\left(\frac{\partial \Psi}{\partial z}\frac{\partial \theta}{\partial x}-\frac{\partial \Psi}{\partial x}\frac{\partial \theta}{\partial z}\right)=\kappa \Delta T\frac{\partial^2 \theta}{\partial x^2}, \tag{26}$$

where $\theta$ is the normalized temperature. From this equation a scale for $\Psi$ is estimated with a scale of the boundary layer $l_s$,

$$\Psi \sim r_c \kappa H/l_s. \tag{27}$$

As pointed out in Section 2, the vorticity equation is essentially in a buoyancy-viscous balance in the side boundary layer:

$$-g\alpha \Delta T\frac{\partial \theta}{\partial x}=\frac{\nu}{r_c}\frac{\partial^4 \Psi}{\partial x^4}. \tag{28}$$

Again, a scale for $\Psi$ is estimated from this equation,

$$\Psi \sim \frac{r_c}{\nu}g\alpha \Delta T\frac{1-\delta\theta}{2}l_s^3, \tag{29}$$

because the radial scale of $\theta$ is $(1-\delta\theta)/2$. Thus the scale $l_s$ is obtained from (27) and (29):

$$l_s=\left(\frac{\nu \kappa H}{g\alpha \Delta T}\frac{2}{1-\delta\theta}\right)^{1/4}. \tag{30}$$

In this relation, dependence of the scale $l_s$ on $\delta\theta$ is smaller than that on $\Delta T$ because $\delta\theta$ is very small compared to 1 in the convection-dominated flow. Therefore we can neglect the dependence on $\delta\theta$. Moreover, considering the fact that an effective width of the boundary layer is several times as large as its scale, we set the width $l$ as follows:

$$l=2\left(\frac{\nu \kappa H}{g\alpha \Delta T}\right)^{1/4}. \tag{31}$$

If we assume the coefficient $1.3|z_1|/B_1$ is 2 in Eq. (9.3) in McIntyre (1968), estimating from his Fig. 6, the same equation corresponding to (31) is obtained.

## References

Fowlis, W.W. and R. Hide, 1965: Thermal convection in a rotating annulus of liquid: effect of viscosity on the transition between axi-symmetric and non-axi-symmetric flow régimes. *J. Atmos. Sci.*, **22**, 541–558.

Held, I.M. and A.Y. Hou, 1980: Nonlinear axially symmetric circulation in a nearly inviscid atmosphere. *J. Atmos. Sci.*, **37**, 515–533.

Hide, R. and P.J. Mason, 1975: Sloping convection in a rotating fluid. *J. Adv. Phys.*, **24**, 47–100.

Hunter, C., 1967: The axi-symmetric flow in a rotating annulus due to a horizontally applied temperature gradient. *J. Fluid Mech.*, **27**, 753–778.

Lorenz, E.N., 1962: Simplified dynamic equations applied to the rotating-basin experiments. *J. Atmos. Sci.*, **19**, 39–51.

Lorenz, E.N., 1963: The mechanics of vacillation. *J. Atmos. Sci.*, **20**, 448–464.

McIntyre, M.E., 1968: The axi-symmetric convective régime for a rigidly bounded rotating annulus. *J. Fluid Mech.*, **32**, 625–655.

Schneider, E.K., 1977: Axially symmetric steady state models of the basic state for instability and climate studies. Part II. Nonlinear calculations. *J. Atmos. Sci.*, **34**, 280–296.

Schneider, E.K. and R.S. Lindzen, 1977: Axially symmetric steady state models of the basic state for instability and climate studies. Part I. Linear calculations. *J. Atmos. Sci.*, **34**, 263–279.

Sugata, S. and S. Yoden, 1991: The effects of centrifugal force on the stability of axi-symmetric viscous flow in a rotating annulus. *J. Fluid Mech.*, **229**, 471–482.

Tokioka, T., 1970: A stability of axi-symmetric flows in a rotating annulus. *J. Meteor. Soc. Japan*, **48**, 293–314.

Williams, G.P., 1967a: Thermal convection in a rotating fluid annulus: part 1. The basic axi-symmetric flow. *J. Atmos. Sci.*, **24**, 144–161.

Williams, G.P., 1967b: Thermal convection in a rotating fluid annulus: part 2. Classes of axi-symmetric flow. *J. Atmos. Sci.*, **24**, 162–174.

# 回転水槽実験における定常軸対称流とその実験パラメータ依存性

菅田誠治・余田成男
(京都大学理学部)

回転水槽中で水平加熱差によって駆動される定常軸対称流を高解像度の二次元非線形数値モデルを用いて求めた。得られた軸対称流の速度場と温度場が実験パラメータにどう依存しているかを広いパラメータ領域で調べた。

定常軸対称流の速度場と温度場が、与えられたパラメータに対してどのように決まるかを直観的に理解できる診断モデルを構築した。モデルは熱伝導が支配的な流れと対流が支配的な流れの両方に適用でき、どのように熱輸送形態が決まるのかを定性的に説明できる。さらに、このモデルを用いて、子午面循環の強さ、東西流の強さ、および内部領域での水平温度差といった、軸対称流を特徴づけるいくつかの量のパラメータ依存性を求めることができる。これらの結果は非線形モデルで得られた結果をうまく説明する。